

# Estimating hysteresis in the soil water retention function from cone permeameter experiments

Jiří Šimůnek

U.S. Salinity Laboratory, ARS, USDA, Riverside, California

Radka Kodešová and Molly M. Gribb

Department of Civil and Environmental Engineering, University of South Carolina, Columbia

Martinus T. van Genuchten

U.S. Salinity Laboratory, ARS, USDA, Riverside, California

**Abstract.** Data obtained from modified cone penetrometer experiments were used to estimate the hysteretic soil hydraulic properties with a parameter estimation technique which combined a numerical solution of the Richards equation with Marquardt-Levenberg optimization. The modified cone penetrometer was designed to inject water into a soil through a cylindrical screen, measure the infiltration rate with time, and track the movement of the wetting front using two tensiometer rings positioned above the screen. After reaching relatively stable tensiometer readings during the experiments, the source of water was cut off and pressure head readings measured while water in the soil profile redistributed. Cumulative inflow and pressure head readings for two experiments with different supply pressures were analyzed to obtain estimates of the soil water retention and hydraulic conductivity functions. Analysis of flow responses obtained during the infiltration period, and of those obtained during the combined infiltration and redistribution phases, demonstrated the importance of hysteresis of the soil hydraulic functions. We found that the redistribution phase could not be described accurately when hysteresis was neglected. Hysteresis in the soil hydraulic functions was modeled using a relatively simple empirical model in which wetting scanning curves are scaled from the main wetting curve and drying scanning curves are scaled from the main drying curve. This model was deemed adequate for our examples. Optimization results for various combinations of unknown soil hydraulic parameters were compared to results of standard laboratory and in situ methods. Estimates of the saturated hydraulic conductivity were well within the range of in situ measurements. The estimated main hysteretic loops of the soil water retention curve were for the most part situated between the wetting and drying curves obtained with standard methods.

## 1. Introduction

Hysteresis can significantly influence water flow and solute transport in variably saturated porous media [e.g., *Vachaud and Thony*, 1971; *Royer and Vachaud*, 1975; *Gillham et al.*, 1979; *Kaluarachchi and Parker*, 1987; *Jaynes*, 1992]. The phenomenon has been observed under both laboratory [e.g., *Topp*, 1969; *Gillham et al.*, 1979] and field [e.g., *Vachaud and Thony*, 1971; *Royer and Vachaud*, 1975; *Watson et al.*, 1975] conditions. The significance of hysteresis has also been demonstrated in several numerical studies [e.g., *Gillham et al.*, 1979; *Kaluarachchi and Parker*, 1987; *Russo et al.*, 1989]. Although long recognized as being important, hysteresis is usually neglected in water flow studies because of a lack of good data.

Hysteresis refers to the nonunique relationship between the pressure head,  $h$ , and the water content,  $\theta$ , in the soil water retention function  $\theta(h)$  (Figure 1). This relationship displays considerable variations in  $\theta$  for the same  $h$  depending upon the

history of soil wetting and drying. During infiltration when the water content and the pressure head are monotonically increasing, the retention curve can be described by a unique function. Similarly, during evaporation or gravity drainage when the water content and the pressure head are monotonically decreasing, the retention curve can also be described by a unique but different function. When drying reverses into a wetting process and vice versa,  $\theta(h)$  is no longer unique and hysteresis must be introduced [*Russo et al.*, 1989]. When the soil is wetted from the residual water content or drained from the saturated water content, the main wetting or drying curves are followed, respectively. When a wetting or drying process is reversed while following the main hysteresis curve, the retention curve follows a primary hysteresis curve. Secondary and higher-order scanning curves are a result of additional reversals [*Jaynes*, 1992; *Kool and Parker*, 1987]. The hysteresis process is described in detail by *Mualem* [1974], *Kool and Parker* [1987], *Luckner et al.* [1989], and *Jaynes* [1992].

Numerous models for describing hysteresis in the soil water retention curve have been developed. Two major groups of models can be distinguished: physically based models and empirical models. Domain models are the most common theoret-

Copyright 1999 by the American Geophysical Union.

Paper number 1998WR900110.  
0043-1397/99/1998WR900110\$09.00

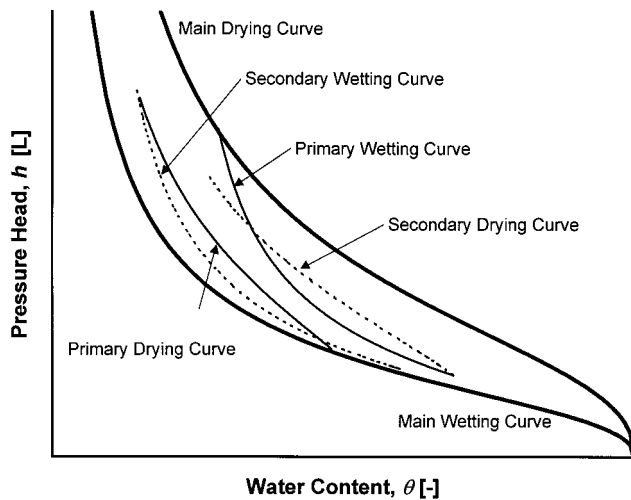


**Figure 1.** Idealized hysteretic soil water retention function showing main, primary, and secondary wetting and drying curves.

ical models. These models divide the soil matrix into a set of pore domains characterized by wetting pore radii that control the filling of pores by water and drying pore radii that control their emptying. A similarity assumption for wetting and drying pore radii [Mualem, 1973, 1974] is often invoked to avoid the requirement for a large number of scanning curves for model calibration. With the similarity assumption, only the main wetting and main drying curves are needed to describe the entire hysteretic phenomenon. Depending on whether pore drainage is assumed to be independent or dependent upon the state of neighboring pores, independent-domain models [Mualem, 1973, 1974] and dependent-domain models [Mualem, 1984a; Mualem and Dagan, 1975] have been developed.

Empirical analytical models assume that the primary, secondary, and higher-order scanning curves can be scaled from the main hysteresis curve [Klute and Heerman, 1974; Hoa et al., 1977; Scott et al., 1983; Kool and Parker, 1987]. Different analytical expressions describing the soil water characteristic curve were used in these studies. Kool and Parker [1987] coupled the analytical model of van Genuchten [1980] with the simplified scaling approach used by Scott et al. [1983] to describe the scanning curves. Scott et al. [1983] assumed that the shape parameters for all drying scanning curves are the same as those for the main drying curve and similarly that the shape parameters for all wetting scanning curves are the same as those for the main wetting curve. Scanning curves are then calculated by varying the residual and saturated water contents for the wetting and drying scanning curves, respectively. Kool and Parker [1987] also assumed that one of the two shape parameters is the same for both wetting and drying, thus decreasing the number of required parameters. An advantage of the model by Scott et al. [1983] is that one can obtain the shape parameters of the drying and wetting curves from knowledge of any main (or primary), secondary, or higher-order scanning drying and wetting curves, respectively.

Most methods for measuring the soil hydraulic properties remain relatively time consuming and costly, are often limited to a relatively narrow range of water contents, and usually pertain to relatively restrictive initial and boundary conditions. Measurement of soil water hysteresis is even more time con-

suming since both water contents and pressure heads must be measured for at least the main drying and wetting curves, and preferably also for additional primary, secondary, and higher-order scanning curves. Generation of a data set suitable for calibrating the domain model of hysteresis can require several months or even years, depending upon whether knowledge of only the main hysteresis loop is needed, or also additional primary and secondary scanning curves. Therefore attempts have been made to develop domain models that require only one branch of the retention curve for calibration of hysteresis. These models, however, have not been found to be very successful [Mualem and Morel-Seytoux, 1978].

A more expedient way for obtaining information about hysteresis in the soil hydraulic properties is to design appropriate transient experiments involving hysteresis and to analyze the data with a suitable inverse procedure. The effort of determining hydraulic properties can thus be shifted from experimentation to computation [Kool and Parker, 1988]. A transient experiment is first carried out with known initial and boundary conditions and subsequently simulated using the governing water flow equation and selected analytical functions representing the soil hydraulic properties. Although the analytical functions must be selected in advance, their parameters are generally unknown. Starting with the initial parameter estimates, the parameters are further adjusted in repeated solutions until deviations between measured and computed water flow attributes (such as water contents, pressure heads, or fluxes) are minimized. The parameter updates can be done manually (trial-and-error calibration) or by using an automated minimization algorithm.

Inverse methods in subsurface hydrology were initially used almost exclusively for saturated flow problems (see the review by Yeh [1986]); they are now also often utilized to analyze unsaturated zone experiments (see the review by Kool et al. [1987]). Parameter estimation techniques were first used with laboratory experiments, such as one-step-type or multistep-type outflow methods [Kool et al., 1985; van Dam, 1992, 1994; Eching and Hopmans, 1993] and evaporation experiments [Cicollaro and Romano, 1995; Santini et al., 1995; Šimůnek et al., 1998], for which the initial and boundary conditions and homogeneity of the soil sample can be readily controlled. The application of inverse methods to field experiments, such as the instantaneous profile method [Dane and Hruska, 1983], disc infiltrometers [Šimůnek and van Genuchten, 1996, 1997], or the extraction method [Inoue et al., 1998], is more complex because of soil heterogeneity and uncertainty associated with the boundary conditions. In addition, field methods have been generally limited to the soil surface or the near surface environment.

A new cone permeameter method currently under development [Gribb, 1996; Gribb et al., 1998; Kodešová et al., 1998a, b] for estimating soil hydraulic properties has the potential for use up to depths of 30 m or more. Cone penetrometers were originally used to obtain soil strength characteristics by measuring the tip resistance and sleeve friction during penetration at a constant rate. To obtain the hydraulic properties, a modified cone penetrometer, instrumented with a porous filter close to the penetrometer tip and two tensiometer rings above the filter, is used. The device is pushed into a soil to the desired depth, and a constant head is applied to the filter. The volume of water imbibed into the soil is monitored during infiltration. The tensiometer rings register movement of the wetting front

during infiltration, as well as the subsequent redistribution process after the source of water has been turned off.

Gribb [1996] gave a detailed numerical analysis of this experiment, including a study of the identifiability of the soil hydraulic parameters. She showed that the inverse solution was most sensitive to the saturated hydraulic conductivity  $K_s$  and the shape parameter  $\alpha$  and least sensitive to the saturated water content  $\theta_s$  and the parameter  $n$  in van Genuchten's [1980] retention function (see equation (10)). The method was recently used to estimate  $K_s$  and the wetting branch of the retention curve of a sandy soil in a laboratory aquifer system [Gribb et al., 1998; Kodešová et al., 1998a, b]. Gribb et al. [1998] also showed that the cone permeameter can be used in fully saturated media to estimate  $K_s$ . Kodešová et al. [1998b] evaluated the effects of cone placement in a soil on the optimized soil hydraulic properties. One set of tests was performed after the cone permeameter was buried in the soil and a second set after the permeameter was pushed to the desired depth. They concluded that for the sandy soil tested, the method of placement had only little impact on the optimized hydraulic parameter values. They also showed that inclusion of the final water content data in the optimization problem improved estimates of  $\theta_s$ . Only the wetting parts of the infiltration experiments were considered in the above mentioned studies.

In this paper we analyze data from both the infiltration and redistribution parts of the experiments utilized by Kodešová et al. [1998b] so as to estimate the hydraulic parameters of both the wetting and drying branches of the soil water retention characteristic. We use only data from two tests performed with the prototype instrument after it was buried (not pushed) in the soil; the tests involved different applied pressure heads but similar initial conditions. The two tests were selected in order to avoid any disturbance of the soil profile caused by cone pushing with concomitant changes in the estimated soil hydraulic parameters. Kodešová et al. [1998b] showed that the observed flow responses could be fit very well with physically reasonable estimates of all optimized hydraulic parameters, with the exception of  $\theta_s$  which was too high for the two examples. For cases in which  $\theta_s$  was fixed at the laboratory-derived value or was reasonably optimized using additional water content data, poorer fits of the measured flow responses were obtained. To improve the solution, we first investigate here the effects of including additional optimized parameters, such as the anisotropy coefficient  $k^A$  and the pore connectivity parameter  $l$  (see equations (3) and (11), respectively), while considering only the infiltration parts of the experiments. The same procedure is then applied to the infiltration and redistribution parts of the experiments with and without consideration of hysteresis. The resulting soil hydraulic characteristics are compared with independently measured laboratory values.

## 2. Theory

### 2.1. Cone Permeameter Experimental Setup: Problem Definition

A cone penetrometer was modified for hydraulic testing. The prototype was discussed in detail by Gribb et al. [1998]. The device consists of four parts: a shaft, a 5-cm screen, and two porous ceramic rings serving as tensiometers located 5 and 9 cm above the screened section (Figure 2). After the cone permeameter is installed in a soil, a constant head is applied to the screen using a microprocessor-controlled solenoid valve assembly. Cumulative flow volume infiltration into the soil

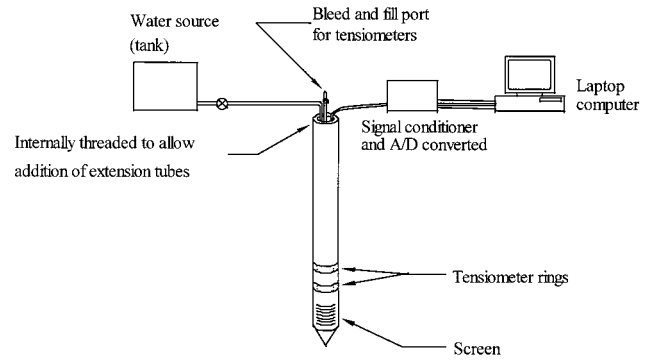


Figure 2. Schematic of the cone permeameter.

through the screen is determined from scale readings of the mass of water removed from a source bottle. The tensiometer rings are connected to pressure transducers to continuously record the transient pore water pressure heads in the soil. Injection of water continues until relatively stable tensiometer readings are reached. The source of water is then cut off, and pressure heads are continuously measured during the ensuing redistribution phase.

Cumulative inflow and pressure head readings are subsequently analyzed to obtain estimates of the soil water retention,  $\theta(h)$ , and hydraulic conductivity,  $K(h)$ , functions. The unknown parameters of  $K(h)$  and  $\theta(h)$  are obtained by minimizing an objective function expressing the difference between measured flow variables and predicted system responses. The system response is modeled by numerical solution of the appropriate governing variably saturated flow equation, augmented with parameterized hydraulic functions and suitable initial and boundary conditions. Initial estimates of the optimized system hydraulic parameters are iteratively improved during the minimization process until a desired degree of precision is obtained.

### 2.2. Governing Variably Saturated Flow Equation

The governing equation for radially symmetric isothermal Darcian flow in a variably saturated anisotropic rigid porous medium is given by the following modified form of Richards' equation:

$$\frac{\partial \theta}{\partial t} = -\frac{1}{r} \frac{\partial (rv_r)}{\partial r} - \frac{\partial v_z}{\partial z} = \frac{1}{r} \frac{\partial}{\partial r} \left( rK \left[ K_{rj}^A \frac{\partial h}{\partial x_j} + K_{rz}^A \right] \right) + \frac{\partial}{\partial z} \left( K \left[ K_{zj}^A \frac{\partial h}{\partial x_j} + K_{zz}^A \right] \right) \quad (1)$$

where  $r$  is the radial coordinate [L];  $z$  is the vertical coordinate positive upward [L];  $t$  is time [T];  $\theta$  is the volumetric water content [ $L^3 L^{-3}$ ];  $v_r$  and  $v_z$  are volumetric fluxes in radial and vertical directions [ $L T^{-1}$ ], respectively;  $h$  is the pressure head [L];  $K_{ij}^A$  are components of a dimensionless anisotropy tensor  $\mathbf{K}^A$ ; and  $K$  is the unsaturated hydraulic conductivity function [ $L T^{-1}$ ] given by

$$K(h) = K_s K_r(h) \quad (2)$$

where  $K_r$  is the relative hydraulic conductivity [-] and  $K_s$  the saturated hydraulic conductivity in the vertical direction [ $L T^{-1}$ ]. The anisotropy tensor  $K_{ij}^A$  in (1) may be used to account for an anisotropic medium. The diagonal entries of  $K_{ij}^A$  are equal to 1 and the off-diagonal entries are equal to zero for an

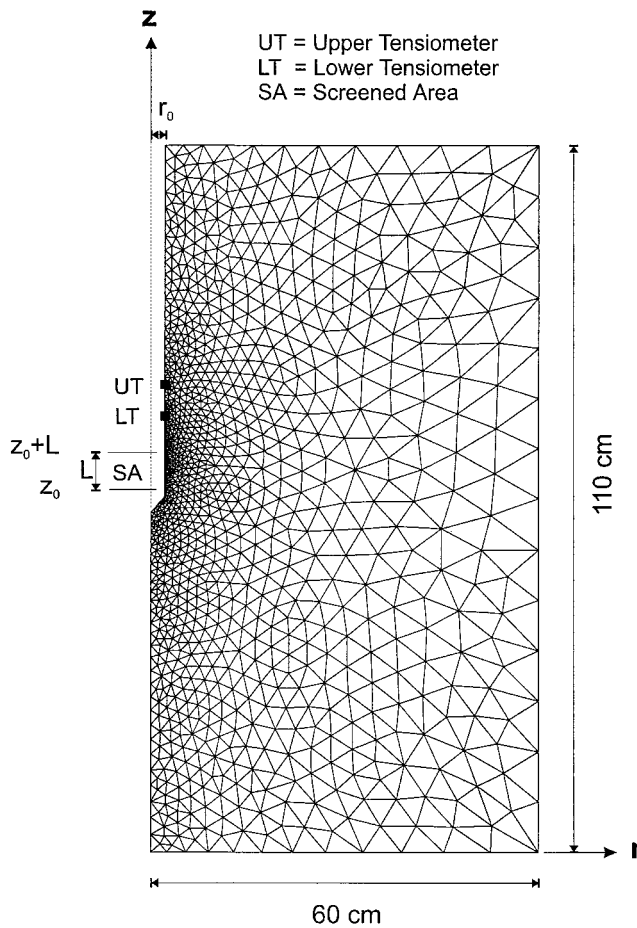


Figure 3. Computational domain and finite element mesh.

isotropic medium. Since in the following we assume that the principal directions of the anisotropy tensor  $\mathbf{K}^A$  coincide with global coordinate system  $(r, z)$ , the off-diagonal entries are equal to 0. The degree of anisotropy can then be represented by an anisotropy coefficient,  $k^A$ , which relates the first and second principal components of the anisotropy tensor  $\mathbf{K}^A$  as follows [Mualem, 1984b]:

$$k^A = K_{rr}^A / K_{zz}^A \quad (3)$$

Assuming that  $K_{zz}^A = 1$ , the anisotropy tensor can be written as

$$\mathbf{K}^A = \begin{bmatrix} k^A & 0 \\ 0 & 1 \end{bmatrix} \quad (4)$$

Equation (1) simplifies to

$$\frac{\partial \theta}{\partial t} = \frac{1}{r} \frac{\partial}{\partial r} \left( r K k^A \frac{\partial h}{\partial r} \right) + \frac{\partial}{\partial z} \left( K \frac{\partial h}{\partial z} + K \right) \quad (5)$$

Notice that we assume that anisotropy is unaffected by the degree of saturation; that is, (3) holds for both saturated and unsaturated soils.

Equation (5) subject to specified initial and boundary conditions is solved numerically using the finite element method for space discretization and finite differences with a fully implicit scheme for temporal discretization [Šimůnek et al., 1996]. A schematic of the transport domain, together with the in-

voked unstructured triangular finite element mesh, is shown in Figure 3.

The solution of (1) for conditions involving hysteresis in soil hydraulic properties requires knowledge of the initial distribution of the pressure head within the flow domain,

$$h(r, z, t) = h_i(r, z) \quad t = 0 \quad (6)$$

where  $h_i$  is the initial pressure head [L], as well as additional information characterizing the history status, that is, information whether the initial condition is on the main drying curve, the main wetting curve, or on a particular scaling curve. The initial water content must also be specified when the initial condition is not on the main wetting or drying branch of the retention curve but inside of the main hysteresis loop.

The boundary condition along the screen section of the cone during infiltration is as follows (Figure 3):

$$h(r, z, t) = h_0(t) - (z - z_0) \quad r = r_0, z_0 < z < z_0 + L \quad (7)$$

where  $h_0$  is the supply pressure head imposed at the bottom of the screen [L],  $z_0$  is the coordinate of the bottom of the screen [L],  $L$  is the length of the screen [L], and  $r_0$  is the radius of the screen [L]. Notice that the supply pressure head,  $h_0$ , can be variable with time;  $h_0$  for our experiment was kept constant during the initial (first) stage of the infiltration process. The cone, however, was still completely filled with water at the moment when the source bottle was disconnected from the permeameter. This water infiltrated during the second stage of the infiltration process, which required us to calculate the supply pressure head from the remaining volume of water in the cone, the geometric characteristics of the interior of the cone body, and the actual infiltration rate. During this second stage of infiltration, the supply pressure head was calculated with

$$h_0(t) = f(V(t)) = f\left(V_0 - \int_{t_0}^t I(t) dt\right) \quad (8)$$

where  $V$  and  $V_0$  are the volumes of water at the current time and at the beginning of the second infiltration stage inside of the cone [L<sup>3</sup>], respectively;  $t_0$  represents the end of the first infiltration stage and start of the second stage [T]; and  $I$  is the actual infiltration rate [L<sup>3</sup> T<sup>-1</sup>]. During each time step the supply pressure head at the screen was kept constant and the infiltration rate corresponding with this Dirichlet-type boundary condition calculated. The volume of water in the cone penetrometer was then correspondingly decreased, thus resulting in the supply pressure head for the new time step. Once all water from the cone had infiltrated, the redistribution stage begins. The following boundary condition then applies along the screen:

$$v_r(r, z, t) = 0 \quad r = r_0, z_0 < z < z_0 + L \quad (9)$$

Other no-flow boundaries are implemented far enough away from the source such that they do not affect water flow during the calculations.

### 2.3. The Unsaturated Soil Hydraulic Properties

We implement the soil hydraulic functions of *van Genuchten* [1980], who used the statistical pore-size distribution model of *Mualem* [1976] to obtain a predictive equation for the unsaturated hydraulic conductivity function in terms of soil water

retention parameters. The expressions of *van Genuchten* [1980] are given by

$$\theta(h) = \begin{cases} \theta_r + \frac{\theta_s - \theta_r}{[1 + |\alpha h|^n]^m} & h < 0 \\ \theta_s & h \geq 0 \end{cases} \quad (10)$$

$$K(h) = K_s S_e^l [1 - (1 - S_e^{1/m})^m]^2 \quad (11)$$

where  $S_e$  is the effective water content [-];  $K_s$  is the saturated hydraulic conductivity [ $L T^{-1}$ ];  $\theta_r$  and  $\theta_s$  denote the residual and saturated water contents [ $L^3 L^{-3}$ ], respectively;  $l$  is a pore-connectivity parameter [-]; and  $\alpha$  [ $L^{-1}$ ],  $n$  [-], and  $m$  ( $= 1 - 1/n$ ) [-] are empirical parameters. The predictive  $K(h)$  model is based on the capillary model of *Mualem* [1976] in conjunction with (10). The above equations contain six independent parameters:  $\theta_r$ ,  $\theta_s$ ,  $\alpha$ ,  $n$ ,  $l$ , and  $K_s$ . The pore-connectivity parameter  $l$  in the hydraulic conductivity function is usually assumed to be 0.5 as an average for many soils [Mualem, 1976].

We incorporated hysteresis by using the empirical model introduced by *Scott et al.* [1983], which assumes that drying scanning curves are scaled from the main drying curve and that wetting scanning curves are scaled from the main wetting curve. This model was also previously employed by *Kool and Parker* [1987], who modified the formulation to account for air entrapment, and by *Vogel et al.* [1996], who also considered hysteresis in the hydraulic conductivity function. The adopted procedure for modeling hysteresis in the retention function requires that both the main drying and main wetting curves be known. These two curves are described with (10) using the parameter vectors  $(\theta_r^d, \theta_s^d, \alpha^d, n^d)$  and  $(\theta_r^w, \theta_s^w, \alpha^w, n^w)$ , where the superscripts  $d$  and  $w$  indicate drying and wetting. The following restrictions are expected to hold in most practical applications:

$$\theta_r = \theta_r^d = \theta_r^w \quad \alpha^d \leq \alpha^w \quad (12)$$

We also invoke the often assumed restriction [Kool and Parker, 1987]

$$n = n^d = n^w \quad (13)$$

so that the parameters  $\theta_s^d$ ,  $\theta_s^w$ ,  $\alpha^d$ , and  $\alpha^w$  are the only independent parameters describing hysteresis in the retention function.

If the main hysteresis loop is not closed at saturation, the water content at saturation for a particular wetting scanning curve can be evaluated using the empirical relationship of *Aziz and Settari* [1979]:

$$\theta_s = \theta_s^d - \frac{\theta_s^d - \theta_{\Delta}}{1 + R(\theta_s^d - \theta_{\Delta})} \quad (14)$$

$$R = \frac{1}{\theta_s^d - \theta_s^w} - \frac{1}{\theta_s^d - \theta_r^d}$$

where  $\theta_{\Delta}$  represents the reversal point. In our analysis, however, we will assume that  $\theta_s = \theta_s^d = \theta_s^w$ , so that the hysteresis retention model is characterized with five parameters ( $\theta_r$ ,  $\theta_s$ ,  $\alpha^d$ ,  $\alpha^w$ ,  $n$ ). With additional three parameters characterizing the conductivity model ( $l$ ,  $k^A$ , and  $K_s$ ), the entire homogeneous system is fully described with eight independent parameters.

The above model of hysteresis may lead to a so called “pumping effect,” which occurs when several drying and wet-

ting cycles result in a considerably lower water content than would be predicted by the domain model of *Mualem* [1984a]. This pumping process is contrary to observed behavior [Jaynes, 1992]. However, “pumping” can become apparent only after several reversals in the wetting and drying cycles and hence should not be important in this study since our experiments involve only one reversal from wetting to drying.

## 2.4. Formulation of the Inverse Problem

The objective function  $\Phi$  to be minimized during the parameter estimation process is formulated using cumulative infiltration data in combination with transient pressure head readings from two tensiometers. The objective function for multiple measurement sets is defined as [Šimůnek and van Genuchten, 1996]

$$\Phi(\mathbf{\beta}, \mathbf{q}_1, \dots, \mathbf{q}_m) = \sum_{j=1}^m \left( v_j \sum_{i=1}^{n_j} w_{i,j} [q_j^*(t_i) - q_j(t_i, \mathbf{\beta})]^2 \right) \quad (15)$$

where  $m$  represents the number of different sets of measurements (cumulative infiltration data and/or tensiometer readings),  $n_j$  is the number of measurements in a particular set,  $q_j^*(t_i)$  are specific measurements at time  $t_i$  for the  $j$ th measurement set,  $\mathbf{\beta}$  is the vector of optimized parameters (e.g.,  $\theta_r$ ,  $\theta_s$ ,  $\alpha^d$ ,  $\alpha^w$ ,  $n$ ,  $l$ ,  $k^A$ , and  $K_s$ ),  $q_j(t_i, \mathbf{\beta})$  are the corresponding model predictions for parameter vector  $\mathbf{\beta}$ , and  $v_j$  and  $w_{i,j}$  are weights associated with a particular measurement set or point, respectively. We assume for now that the weighting coefficients  $w_{i,j}$  in (15) are equal to 1, that is, the variances of the errors inside a particular measurement set are assumed the same. The weighting coefficients  $v_j$ , which minimize differences in weighting between different data types because of different absolute values and numbers of data involved, are given by [Clausnitzer and Hopmans, 1995]

$$v_j = \frac{1}{n_j \sigma_j^2} \quad (16)$$

thus defining the objective function as the average weighted squared deviation normalized by measurement variances  $\sigma_j^2$ .

Minimization of the objective function  $\Phi$  is accomplished by using the Levenberg-Marquardt nonlinear minimization method [Marquardt, 1963]. This method was found to be very effective and has become a standard in nonlinear least squares fitting among soil scientists and hydrologists [van Genuchten, 1981; Kool et al., 1985, 1987; Šimůnek and van Genuchten, 1996].

## 3. Methods

### 3.1. The Laboratory Aquifer

Cone tests were carried out in a laboratory aquifer measuring  $4.7 \times 4.7 \times 2.6$  m. The aquifer material was a sandy soil with occasional kaolin pockets, underlain by 20 cm of gravel. The bulk density of undisturbed soil samples ranged from 1.65 to 1.69  $g\ cm^{-3}$ . The soil hydraulic properties were determined using several standard methods. The wetting branch of the retention curve was obtained by capillary rise tests [Lambe, 1951] and a computer-automated extraction/sorption laboratory testing method [Znidarčič et al., 1991; Ray and Morris, 1994]. The drainage branch was measured with pressure plate tests. The pressure plate and the computer-automated tests

**Table 1.** Hydraulic Parameters Obtained From Various Laboratory Tests

Test	$\alpha^w$ , cm <sup>-1</sup>	$\alpha^d$ , cm <sup>-1</sup>	$n$ [-]	$\theta_r$ [-]	$\theta_s$ [-]	$K_s$ , cm s <sup>-1</sup>
Capillary rise	0.0864	...	3.60	0.008	0.329	...
Computer-automated	0.139	...	2.17	0.042	0.345	...
Pressure plate method	...	0.045	1.61	0.008	0.35	...
Constant head laboratory	...	...	...	...	...	0.00385
Slug	...	...	...	...	...	0.00725
Guelph permeameter	...	...	...	...	...	0.00349
Cone permeameter (saturated conditions)	...	...	...	...	...	0.0134

were performed on undisturbed samples, while the capillary rise tests were carried out on repacked samples. The soil hydraulic parameters for both branches of the retention curve were obtained by fitting (10) to  $\theta(h)$  data using the RETC code [van Genuchten et al., 1991]. Soil hydraulic parameters determined with the different laboratory methods are presented in Table 1.

A series of drive tube samples was taken from the testing area and subjected to laboratory constant head permeability tests. Besides the laboratory tests, slug tests and Guelph permeameter tests were performed in the laboratory aquifer in other studies [Scaturo, 1993; Singleton, 1997]. Slug test data were analyzed using the Bower and Rice [1976] equation, while Guelph permeameter data were analyzed according the method of Reynolds [1993]. The saturated hydraulic conductivity was also estimated using Hvorslev's [1951] analytical equation adopted for infiltration from a cone penetrometer into a saturated soil [Gribb et al., 1998]. Table 1 summarizes  $K_s$  values obtained with the various methods.

### 3.2. Cone Penetrometer Tests

The cone penetrometer was placed in a hole in the laboratory aquifer and the soil around the cone was backfilled such that the center of the screened section was 65 cm below the soil surface. This method of placement ensured relative homogeneity of the soil surrounding the prototype without possible soil disturbance due to pushing the cone to the testing depth. The water table in the laboratory aquifer was raised to ground surface and then lowered first to 26 and then to 48 cm below the surface of the aquifer. Under these conditions the cone was used as a piezometer to obtain saturated hydraulic conductivity values [Gribb et al., 1998]. The water table was subsequently lowered to approximately 190 cm below the soil surface to establish unsaturated conditions in the aquifer. This depth ensured that tests would not be influenced by the presence of a water table. The laboratory aquifer was left undisturbed for 2 weeks before running the first infiltration test. The second infiltration test was performed about 3 weeks after the first one using the same experimental setup. We selected these two infiltration tests for further analysis.

During experiment 1 a supply pressure ( $h_0$ ) of 52.5 cm was applied at the bottom of the screen for a period of 400 s ( $0 < t < 400$  s), while a pressure of 32.5 cm was applied for 445 s during the experiment 2. The total volumes of water infiltrated during experiments 1 and 2 were 11.2 and 6.95 l, respectively. Tensiometer readings were obtained for 840 s ( $0 < t < 840$  s). Initial pressure heads of the upper tensiometer were approximately equal to  $-50$  cm for both tests. This relatively low pressure head corresponds to less than 10% of the effective saturation value for this particular soil; the experiment hence covered more than 90% of the range of saturation. Pressure

heads of the upper tensiometer at the end of the infiltration period were  $-16$  and  $-18$  cm and dropped to about  $-34$  and  $-32$  cm at the end of the experiments. The data collected for both tests are shown in Figure 4. Although measurements were recorded every second, only data collected at 5-s intervals were included in objective function (15).

### 3.3. Numerical Inversions

Table 2 summarizes the different numerical inversions carried out on both data sets. The first five inversions (set 1, runs 1–5) analyzed only the first infiltration stage for both experiments to obtain estimates of the wetting branches of soil hydraulic properties. Hysteresis was not considered in these runs. In the first five inversions we optimized the parameters  $\alpha^w$ ,  $n$ , and  $K_s$  alone or together with different combinations of the parameters  $\theta_s$ ,  $l$ , and  $k^A$ . Using numerically generated data, Gribb [1996] showed that the inversion procedure is very insensitive to the saturated water content  $\theta_s$ , which is the reason why we fixed this parameter in several optimizations at a value of 0.35. This value was selected on the basis of calculations from the bulk density and results of laboratory tests (Table 1). Unless optimized, the parameter  $l$  was assumed to be equal to 0.5 [Mualem, 1976], while the anisotropy coefficient  $k^A$  was set equal to 1.0. The residual water content was always equated to the value obtained from capillary rise experiments ( $\theta_r = 0.008$ ), since we did not expect this parameter to be identifiable from the near-saturated experiments. The first five inversions (set 1) were repeated using measured data from the entire experiments, that is, using both the infiltration and redistribution data. Hysteresis again was neglected in these optimizations.

The next eight optimizations (set 2, runs 6–13) involved data entirely from experiments 1 and 2 and considered hysteresis in the soil hydraulic properties. These data sets contained information about both wetting and drying and about the corresponding branches of the soil hydraulic properties. Again, the parameters  $\alpha^w$ ,  $n$ , and  $K_s$  were optimized in all eight inversions. The parameter  $\alpha^d$  was either optimized independently or assumed coupled with  $\alpha^w$  by the relationship

$$\alpha_w = 2\alpha_d \quad (17)$$

which is often used as a reasonable approximation [Kool and Parker, 1987; Nielsen and Luckner, 1992]. Again, the parameters  $\theta_s$ ,  $l$ , and  $k^A$ , with or without a combination of  $\theta_s$  and  $l$  were optimized in the numerical inversions. Parameter constraints had to be specified to avoid numerical instabilities for high values of  $n$  and  $l$  ( $n \in [1.1, 7.5]$ ,  $l \in [-20, +20]$ ). Constraints were also imposed on  $\theta_s$  ( $\theta_s \leq 0.6$ ) to avoid physically unrealistic values. The initial estimates of the soil hydraulic parameters in most inversions were as follows:  $\theta_s =$

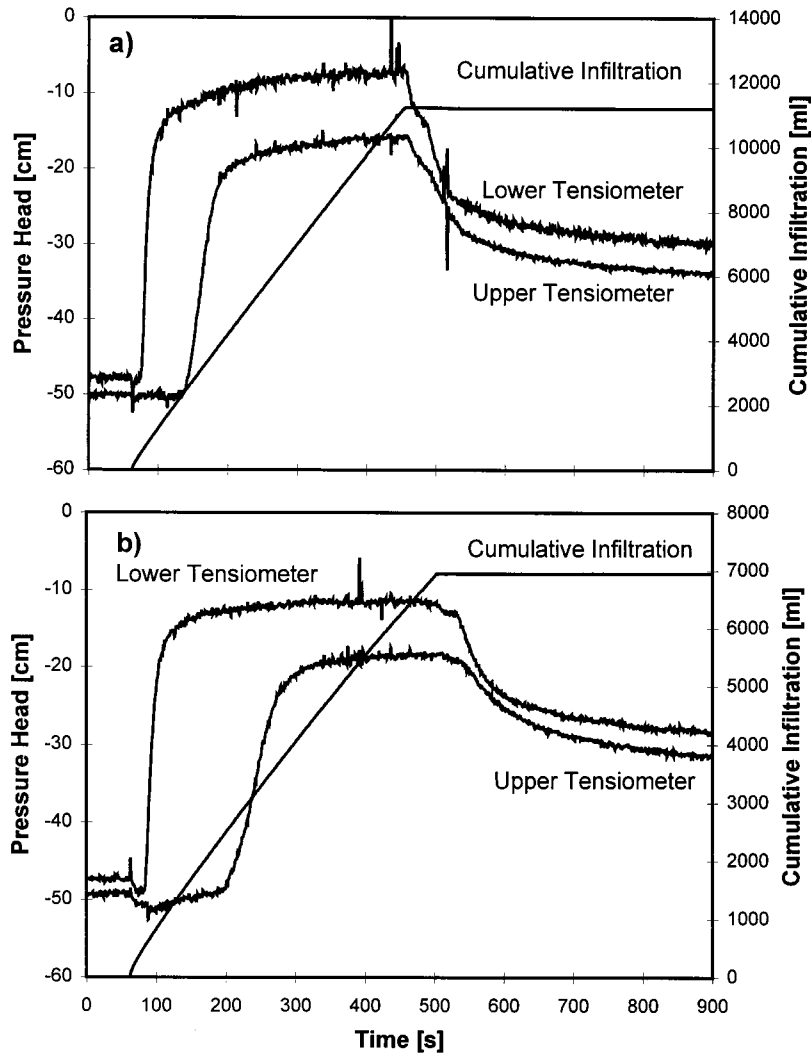


Figure 4. Experimental data for (a) experiment 1 and (b) experiment 2.

0.35,  $\alpha^d = 0.3$ ,  $\alpha^w = 0.5$ ,  $n = 4.0$  (6.0),  $l = 0.5$ ,  $k^A = 1.0$ , and  $K_s = 0.01$ . Variances of all measured values of pressure heads and cumulative infiltration volumes were used as measurement variances in (16).

Depending upon the wetting or drying history of a soil, a wide range of water contents can be associated with a particular measured pressure head. If no information about both the initial water contents and the initial pressure heads is available,

Table 2. Summary of Optimization Runs

Run	Hysteresis	$\theta_s$	$\alpha^w$	$n$	$K_s$	$l$	$k^A$	$\alpha^d$
<i>Set 1</i>								
1	no	0.35	opt	opt	opt	0.5	1.0	NA
2	no	opt	opt	opt	opt	0.5	1.0	NA
3	no	0.35	opt	opt	opt	0.5	opt	NA
4	no	0.35	opt	opt	opt	opt	1.0	NA
5	no	opt	opt	opt	opt	opt	1.0	NA
<i>Set 2</i>								
6	yes	opt	opt	opt	opt	0.5	1.0	opt
7	yes	opt	opt	opt	opt	0.5	1.0	opt <sup>a</sup>
8	yes	0.35	opt	opt	opt	0.5	opt	opt
9	yes	0.35	opt	opt	opt	0.5	opt	opt <sup>a</sup>
10	yes	0.35	opt	opt	opt	opt	1.0	opt
11	yes	0.35	opt	opt	opt	opt	1.0	opt <sup>a</sup>
12	yes	opt	opt	opt	opt	opt	1.0	opt
13	yes	opt	opt	opt	opt	opt	1.0	opt <sup>a</sup>

Numbers represent fixed parameters. Opt, optimized.

<sup>a</sup>Optimized as  $\alpha^w = 2\alpha^d$ .

**Table 3.** Results of Numerical Inversions for Experiment 1 Without Considering Hysteresis

Run	$\Phi$	$\theta_s$ [-]	$\alpha^w$ , cm <sup>-1</sup>	$n$ [-]	$K_s$ , cm s <sup>-1</sup>	$l$ [-]	$k^A$ [-]	$\alpha^d$ , cm <sup>-1</sup>	Rank
<i>Fitted to Only Infiltration Data</i>									
1	0.0604	...	0.045	5.76	0.0114	...	...	...	5
2	0.00877	0.459	0.0520	6.77	0.0119	...	...	...	2
3	0.00879	...	0.0527	6.11	0.00965	...	1.37	...	3
4	0.00956	...	0.0357	6.05	0.0119	14.2	...	...	4
5	0.00839	0.405	0.0442	5.42	0.0119	2.28	...	...	1
<i>Fitted to Infiltration and Redistribution Data</i>									
1*	0.0986	...	0.0349	4.02	0.0115	...	...	...	5
2*	0.0777	0.600 <sup>a</sup>	0.0297	2.34	0.0122	...	...	...	3
3*	0.0708	...	0.0329	2.42	0.00764	...	1.96	...	2
4*	0.0820	...	0.0288	5.41	0.013	10.6	...	...	4
5*	0.0475	0.600 <sup>a</sup>	0.0268	3.22	0.0118	4.65	...	...	1

<sup>a</sup>Upper parameter constraint.

then this possible variation in water content must be considered in the optimization process. Therefore, set 2 inversions were carried out twice. We first assumed that the initial condition was derived from the main wetting branch of the retention curve and next from the main drying branch. In general, a soil will be at a scanning curve in between the main wetting and main drying branches. In this way, both extremes of the initial conditions are hence considered.

## 4. Results and Discussion

### 4.1. Analysis of the Infiltration Process

Results of the numerical inversions for experiments 1 and 2, without considering hysteresis, are summarized in Tables 3 and 4, respectively. The first five runs in each table used only infiltration data, while the second set of runs (runs 1\* through 5\*) used both infiltration and redistribution data. In addition the optimized parameters, Tables 3 and 4 give also the final values of the objective function and a ranking for each run (1 being the best). The rankings presented here are based solely on the final value of the objective function and do not consider the number of optimized parameters, the accuracy of their prediction, or any other criteria involving uniqueness of the optimization results. Hence inversions with a higher number of optimized parameters are ranked higher than those with fewer optimized parameters. We emphasize that the rankings in Tables 3–8 serve only to simplify interpretation of the results. Parameters not given for a particular numerical inversion (e.g.,  $\theta_r$ ,  $\theta_s$ ,  $\alpha^d$ ,  $l$ ,  $k^A$ ) were fixed and are given in Table 2.

Measured and optimized cumulative infiltration volumes and pressure heads resulting from the first five numerical inversions are plotted in Figure 5. Measured pressure heads and cumulative infiltration volumes were not well described when  $\theta_s$  was fixed and only three parameters ( $\alpha^w$ ,  $n$ , and  $K_s$ ) were optimized (run 1). The model predicted an earlier arrival of the wetting front at both tensiometers than actually observed and also underestimated the cumulative infiltration volume for both experiments. Improved fits could be obtained by optimizing  $\theta_s$ , the anisotropy factor  $k^A$ , and/or the tortuosity factor  $l$  (runs 2–5 in Tables 3 and 4). Results show that optimization of  $\theta_s$ ,  $k^A$ , and  $l$ , or  $\theta_s$  and  $l$ , along with  $K_s$ ,  $\alpha$ , and  $n$  yielded almost identical flow responses (Figure 5). The very similar final values of the objective function (Tables 3 and 4) for runs 2–5 make it impossible to clearly distinguish between the effects of the different parameters. The estimated value of  $\theta_s$  (run 2) was greater than 0.35 (the value estimated from laboratory soil bulk density and water content measurements) and provided increased infiltration capacity. The optimized value of the anisotropy coefficient  $k^A$  (run 3) was greater than 1 (the value associated with isotropic flow), leading to more flow in the radial direction and, indirectly, also more infiltration. The fitted value of the pore-connectivity parameter  $l$  (run 4) was greater than the 0.5 and resulted in a faster decrease of the hydraulic conductivity with decreasing water content. This feature yielded a much sharper wetting front. Finally, the simultaneous optimization of  $\theta_s$  and  $l$  (run 5) generated values that were greater than 0.35 and 0.5, respectively, but lower than values resulting from runs 2 and 4, respectively.

**Table 4.** Results of Numerical Inversions for Experiment 2 Without Considering Hysteresis

Run	$\Phi$	$\theta_s$ [-]	$\alpha^w$ , cm <sup>-1</sup>	$n$ [-]	$K_s$ , cm s <sup>-1</sup>	$l$ [-]	$k^A$ [-]	$\alpha^d$ , cm <sup>-1</sup>	Rank
<i>Fitted to Only Infiltration Data</i>									
1	0.0460	...	0.0501	6.36	0.00900	...	...	...	5
2	0.00588	0.430	0.0570	7.50 <sup>a</sup>	0.00951	...	...	...	4
3	0.00551	...	0.0577	7.50 <sup>a</sup>	0.00810	...	1.27	...	3
4	0.00456	...	0.0486	6.71	0.00952	2.71	...	...	1
5	0.00456	0.350	0.0486	6.72	0.00952	2.69	...	...	2
<i>Fitted to Infiltration and Redistribution Data</i>									
1*	0.1007	...	0.0406	4.74	0.00889	...	...	...	5
2*	0.0754	0.497	0.0396	3.00	0.00966	...	...	...	3
3*	0.0777	...	0.0410	3.01	0.00741	...	1.48	...	4
4*	0.0447	...	0.0288	5.00	0.00912	19.5	...	...	2
5*	0.0260	0.848	0.0208	2.75	0.00976	20.0 <sup>a</sup>	...	...	1

<sup>a</sup>Upper parameter constraint.

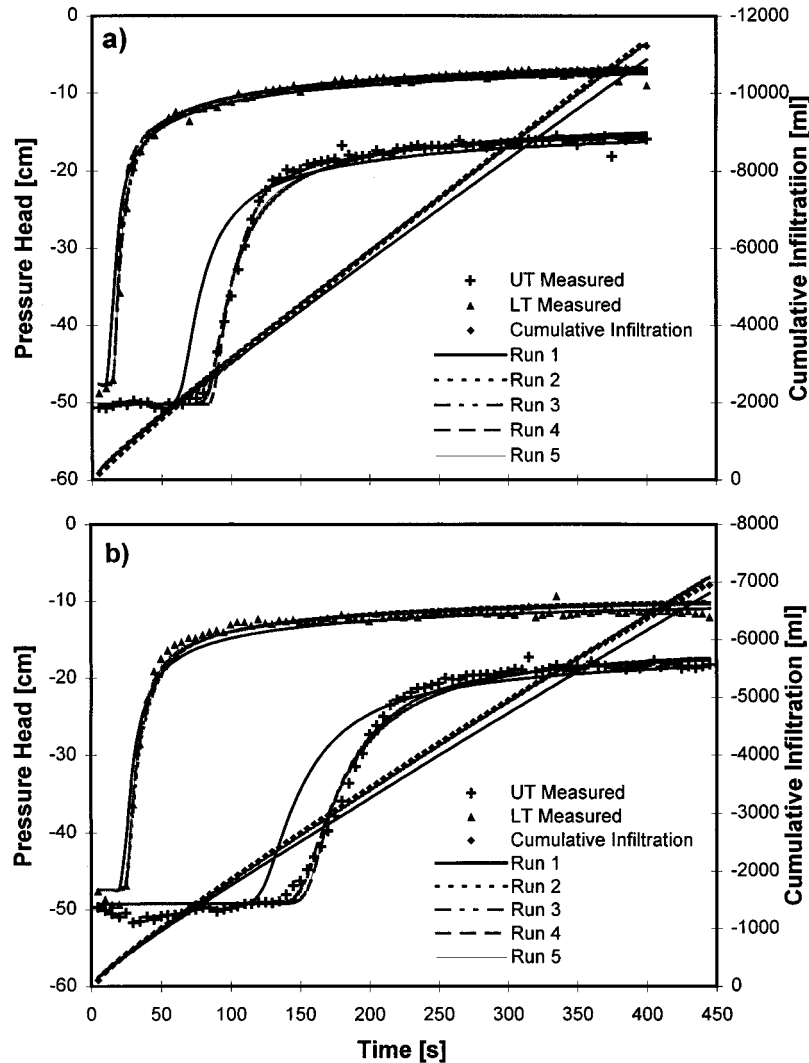


**Figure 5.** Measured and optimized pressure heads and cumulative infiltrations for (a) experiment 1 and (b) experiment 2 during the first infiltration stage.

Despite differences in the sets of optimized parameters, as discussed above, the other simultaneously fitted parameters ( $\alpha^w$ ,  $n$ , and  $K_s$ ) showed remarkable consistency among the optimization runs. The optimized  $K_s$  value ranged from 0.00965 to 0.0119  $\text{cm s}^{-1}$  and from 0.00810 to 0.00952  $\text{cm s}^{-1}$  for experiments 1 and 2, respectively, while values of  $\alpha^w$  ranged from 0.0357 to 0.0527  $\text{cm}^{-1}$  and from 0.0484 to 0.0577  $\text{cm}^{-1}$ , and those of  $n$  between 5.42 and 6.77 and between 6.36 and 7.50, for experiments 1 and 2, respectively. On the basis of a numerical ranking of the value of the objective function and considering the values of optimized parameters, the best solution seems to be run 5 with  $\theta_s$  and  $l$  as additional fitting parameters.

The parameters optimized for the infiltration process were next used to predict observed pressure heads for the redistribution phase of the experiment. Hysteresis was either neglected ( $\alpha^d = \alpha^w$ ) or considered ( $\alpha^d = \alpha^w/2$ ) using the simplifying assumption of (17). A comparison of calculated and measured pressure heads at lower tensiometer for experiment 1 is shown in Figure 6a. This figure clearly shows that although the infiltration part of the experiment was fitted very successfully, the resulting optimized parameters could not be used to describe the redistribution stage. Measured pressure

heads decreased much faster and dropped to lower values than those simulated when hysteresis was neglected. On the other hand, considering hysteresis with the simplifying assumption of (17) resulted in calculated pressure heads that decreased faster than the measured values. Measured pressure heads were always in between those predicted with and without hysteresis. Similar results were also obtained for experiment 2 (Figure 6b). Values for the objective function  $\Phi$  for optimizations using infiltration data only but which applied to the entire experiment, were very high for all cases (between 0.2 and 0.9), as could be expected from inspection of Figure 6.

#### 4.2. Simultaneous Analysis of Infiltration and Redistribution Data

The soil hydraulic parameters were next estimated using data from both the infiltration and redistribution phases for cases in which (1) hysteresis was neglected, (2) hysteresis was considered with the parameters  $\alpha^d$  and  $\alpha^w$  being fitted independently, and (3) hysteresis was considered but restricted to the simplifying assumption (17). Two different runs were executed for each case with hysteresis: one set assuming that the water content corresponding to the initial pressure heads could be

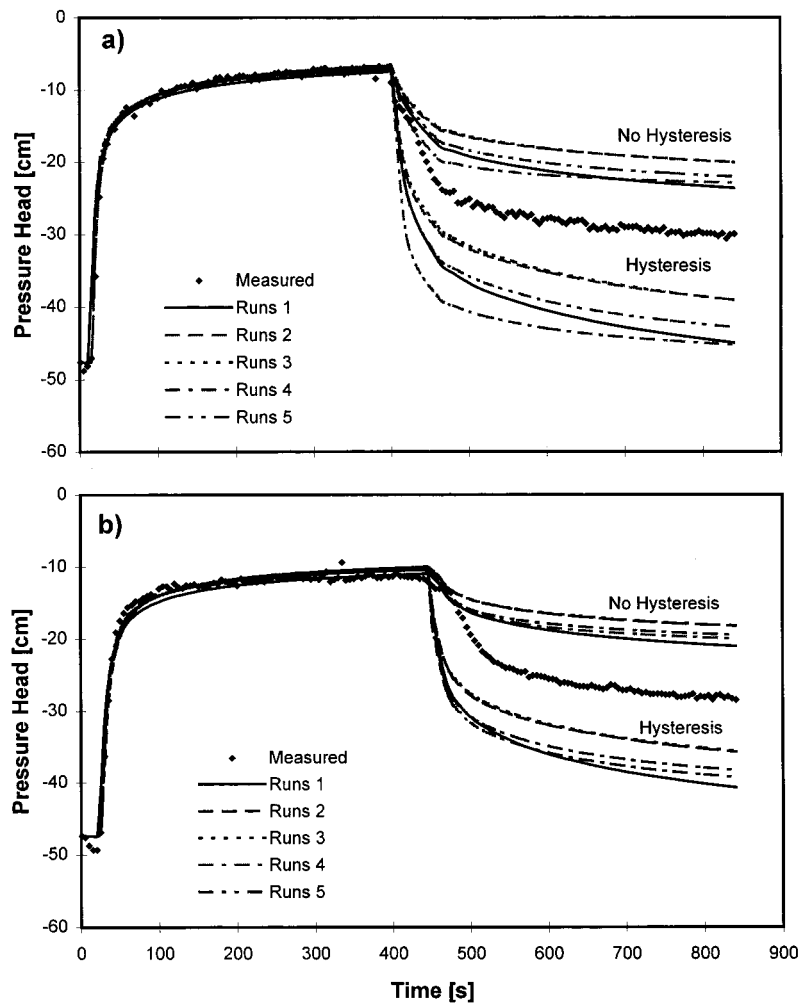


**Figure 6.** Measured and optimized pressure heads at the lower tensiometer for (a) experiment 1 and (b) experiment 2 during both infiltration and redistribution. The input parameters were optimized using infiltration data only. The redistribution stage was simulated with ( $\alpha^w = 2\alpha^d$ ) or without ( $\alpha^w = \alpha^d$ ) hysteresis.

taken from the main wetting branch and a second set assuming that the initial condition was given by the main drying branch.

Results for cases when hysteresis was not considered are summarized in Tables 3 and 4, and the measured and simulated flow responses are shown in Figure 7. A relatively good agreement between measured and calculated cumulative infiltration volumes was obtained for both experiments. The overall fit of the measured pressure head was better than that shown in Figure 6, where the redistribution phase was predicted using wetting branch hydraulic data. Calculated pressure heads during the final stages of wetting were generally lower, and those during redistribution generally higher, than the measured values, while the wetting front reached the tensiometers earlier than observed. Although values of the objective function were much lower than those for simulations presented in Figure 6, this was often achieved with physically unreasonable parameter values (see, for example,  $\theta_s$  and  $l$  for runs 4\* and 5\*). Although still relatively small, the optimized  $K_s$  now also shows a broader range of values (0.00764–0.013 cm s<sup>-1</sup> and 0.00741–0.00976 cm s<sup>-1</sup> for experiments 1 and 2, respectively) as compared to those derived from infiltration only. The values of  $\alpha^w$  (0.0265–0.0349 cm<sup>-1</sup> and 0.0208–0.0410 cm<sup>-1</sup>) and  $n$  (2.34–5.41 and 2.78–5.00) estimated from

the combined infiltration and redistribution process are now considerably lower than those obtained from the infiltration data only. The lower  $n$  values reflect the inability of the numerical model to predict the sharp moisture fronts at both tensiometers. The need to simulate a sharp wetting front consequently resulted in extremely high values of  $l$  for runs 4\* and 5\*.

Results of the optimizations using the hysteretic hydraulic property model with initial conditions defined by the wetting branch of the retention curve are presented in Figure 8 and Tables 5 and 6. As before, only values of the optimized parameters are shown in the tables. All optimizations allowing for an independent fit of  $\alpha^d$  and  $\alpha^w$  (runs 6, 8, 10, and 12) resulted in excellent agreement between measured and calculated pressure heads and cumulative infiltration volumes for both experiments. Both the arrival and the shape of the wetting front, as well as the decline of pressure heads during redistribution, were now captured with remarkable accuracy. Small discrepancies between the measured and optimized pressure heads were present during the second stage of infiltration after the cone was disconnected from the source bottle and only water remaining in the cone body continued to infiltrate through the screen (before the redistribution stage started). This second infiltration stage, lasting between 35 and 40 s, may

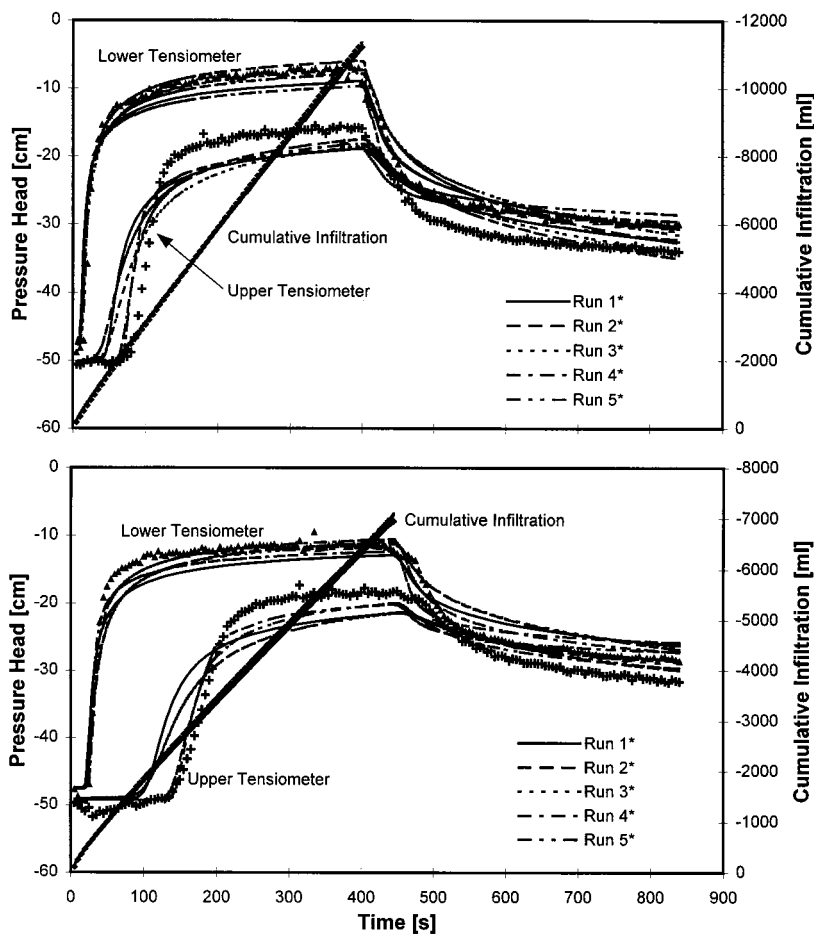


**Figure 7.** Measured and optimized pressure heads and cumulative infiltration for experiment 1 (top) and experiment 2 (bottom) during both infiltration and redistribution. Hysteresis was not considered.

not have been properly characterized in the numerical solution. Some additional water, perhaps from the water supply tube, may not have been accurately accounted for by boundary condition (8). When optimized,  $\theta_s$  values again were overpredicted, perhaps suggesting some anisotropy of the soil or a sharper decrease in the hydraulic conductivity function with decreasing pressure head as reflected by a higher value of  $l$ . Even with these uncertainties related to  $\theta_s$ ,  $k^A$ , and  $l$ , the other soil hydraulic parameters ( $\alpha$ ,  $n$ ,  $K_s$ ) remained exceptionally consistent among the various optimization runs. For example,  $K_s$  was predicted to be in the range of 0.00971–0.0120 cm s<sup>-1</sup> for experiment 1 and 0.0834–0.00969 for experiment 2. The parameters  $\alpha^d$  and  $\alpha^w$  for runs 6, 8, and 12 ranged from 0.0325 to 0.0328 cm<sup>-1</sup> and from 0.0499 to 0.0515 for experiment 1 and from 0.0359 to 0.0368 and from 0.0500 to 0.0559 for experiment 2, and slightly lower for run 10. The parameter  $n$  was predicted to be within the narrow intervals of 5.27–5.61 and 4.75–5.59 for the two experiments. All of these intervals are remarkably narrow considering the relatively high sensitivity of the parameter estimation technique.

The numerical solutions obtained with optimizations constrained by (17) ( $\alpha^w = 2\alpha^d$ ) (runs 7, 9, 11, and 13) generally underpredicted the cumulative infiltration volumes as well as the pressure heads during infiltration. However, the redistribution phase was described equally well as when  $\alpha^d$  and  $\alpha^w$  were both optimized. The final values of the objective functions

when both  $\alpha^d$  and  $\alpha^w$  were optimized were, on average, about half of those obtained when constraint (17) was invoked. Although  $\alpha^w$  and  $K_s$  were again found to be within relatively narrow intervals (0.0583–0.0674 cm<sup>-1</sup> and 0.00923–0.0123 cm s<sup>-1</sup> for experiment 1 and 0.0674–0.0753 and 0.00838–0.0102 for experiment 2),  $n$  became then unreasonably high, as it often reached the upper constraint of 7.50 imposed to avoid numerical instabilities.

Results of the optimizations using the hysteretic model and the initial condition defined by the drying branch of the retention curve are presented in Figure 9 and Tables 7 and 8. These inverse solutions now returned higher initial water contents than was the case with the initial condition given by the wetting branch. Since all other water flow attributes were similar, the higher initial water contents resulted in higher optimized  $\theta_s$  values as well. However, when  $\theta_s$  was fixed at 0.350, the numerical inversions yielded (as expected) higher values of the anisotropy coefficient  $k^A$  and exponent  $l$ . Values of the other optimized parameters ( $\alpha^w$ ,  $\alpha^d$ ,  $n$ , and  $K_s$ ) remained almost the same as those obtained when the wetting branch was used for the initial condition. Again, we obtained excellent correspondence between measured and calculated values of the pressure head and the cumulative infiltration volume when  $\alpha^w$  and  $\alpha^d$  were fitted independently. When  $\alpha^w$  and  $\alpha^d$  were constrained by (17), the predicted pressure heads during the infiltration phase were again underpredicted, except for run 11 of experiment 1.

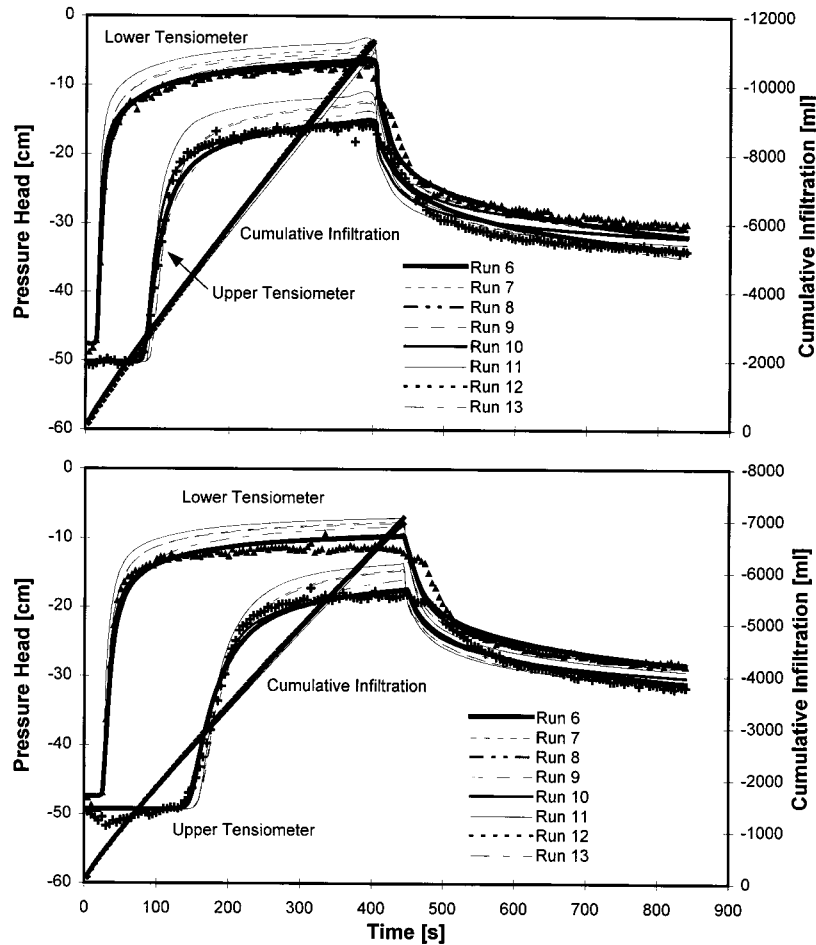


**Figure 8.** Measured and optimized pressure heads and cumulative infiltration for experiment 1 (top) and experiment 2 (bottom) during both infiltration and redistribution. Hysteresis was considered; the initial condition was assumed to be on a main wetting branch of the retention curve.

#### 4.3. Comparison of Optimized and Independently Measured Soil Hydraulic Properties

Figure 10 compares the estimated and independently measured soil water retention functions, as well as estimated hydraulic conductivity functions, for experiment 1 (optimizations from infiltration data only). Retention curves (Figure 10a) obtained by parameter estimation resembled fairly closely the experimental laboratory wetting curves determined with the capillary rise (CR) and computer-automated (CA) methods. The main deviations involve sharp decreases in estimated

water contents away from saturation at low suction values. Desaturation occurred at somehow higher tensions than expected from the laboratory test results. Notice that the inverse solutions for different combinations of optimized parameters all yielded quite similar retention curves, except near saturation. Differences near to saturation are primarily due to uncertainty in the estimated  $\theta_s$  values (see also Table 3).

Differences between the various optimized hydraulic conductivity functions (Figure 10b) obtained in this work are also

**Table 5.** Results of Numerical Inversions for Experiment 1 Considering Hysteresis With Initial Conditions Assumed From the Wetting Curve

Run	$\Phi$	$\theta_s$ [-]	$\alpha^w$ , cm <sup>-1</sup>	$n$ [-]	$K_s$ , cm s <sup>-1</sup>	$l$ [-]	$k^A$ [-]	$\alpha^d$ , cm <sup>-1</sup>	Rank
6	0.0125	0.453	0.0499	5.35	0.0120	...	...	0.0325	2–3
7	0.0331	0.498	0.0640	7.50 <sup>a</sup>	0.0123	...	...	...	7
8	0.0122	...	0.0515	5.27	0.00971	...	1.37	0.0328	1
9	0.0291	...	0.0652	7.50 <sup>a</sup>	0.00923	...	1.52	...	6
10	0.0225	...	0.0389	5.61	0.0118	6.25	...	0.0287	5
11	0.0863	...	0.0583	7.50 <sup>a</sup>	0.0122	5.01	...	...	8
12	0.0125	0.453	0.0501	5.41	0.0120	0.480	...	0.0325	2–3
13	0.0169	0.663	0.0674	7.50 <sup>a</sup>	0.0119	0.710	...	...	4

<sup>a</sup>Upper parameter constraint.

**Table 6.** Results of Numerical Inversions for Experiment 2 Considering Hysteresis With Initial Conditions Assumed From the Wetting Curve

Run	$\Phi$	$\theta_s$ , [-]	$\alpha^w$ , $\text{cm}^{-1}$	$n$ [-]	$K_s$ , $\text{cm s}^{-1}$	$l$ [-]	$k^A$ [-]	$\alpha^d$ , $\text{cm}^{-1}$	Rank
6	0.0128	0.423	0.0553	5.59	0.00966	...	...	0.0364	3
7	0.0384	0.443	0.0712	7.45	0.0101	...	...	...	7
8	0.0124	...	0.0559	5.31	0.00834	...	1.25	0.0368	2
9	0.0371	...	0.0722	7.50 <sup>a</sup>	0.00838	...	1.33	...	6
10	0.0130	...	0.0438	4.75	0.00967	3.58	...	0.0329	4
11	0.0654	...	0.0674	6.72	0.0102	2.08	...	...	8
12	0.0122	0.389	0.0500	4.94	0.00969	1.35	...	0.0359	1
13	0.0229	0.615	0.0753	7.50 <sup>a</sup>	0.00981	-0.577	...	...	5

<sup>a</sup>Upper parameter constraint.

relatively small and would be acceptable for most practical applications. Hydraulic conductivities at or near saturation vary only by about 20%. The largest deviations occurred for the optimization run considering anisotropy when the saturated hydraulic conductivity in the vertical direction,  $K_s^v$ , was smaller than those obtained with the other runs. On the other hand, the estimated saturated hydraulic conductivity in the radial direction,  $K_s^r$ , was somewhat higher than those determined with other methods. The optimized  $K_s$  values were on average only about 15% and 40% smaller for experiments 1 and 2, respectively, than  $K_s$  values determined from a slug test per-

formed with the cone penetrometer at the same location (Table 1). Numerically estimated values of  $K_s$  were approximately 50% and 25% higher than those obtained with the slug test, respectively. Finally, inverse solutions of the cone penetrometer test gave hydraulic conductivities which were approximately three times larger than those determined with the constant head laboratory and Guelph permeameter tests.

Figures 11 and 12 present for experiments 1 and 2, respectively, the estimated and measured soil water retention and estimated hydraulic conductivity functions obtained using data from the entire cone penetrometer test (infiltration plus redi-

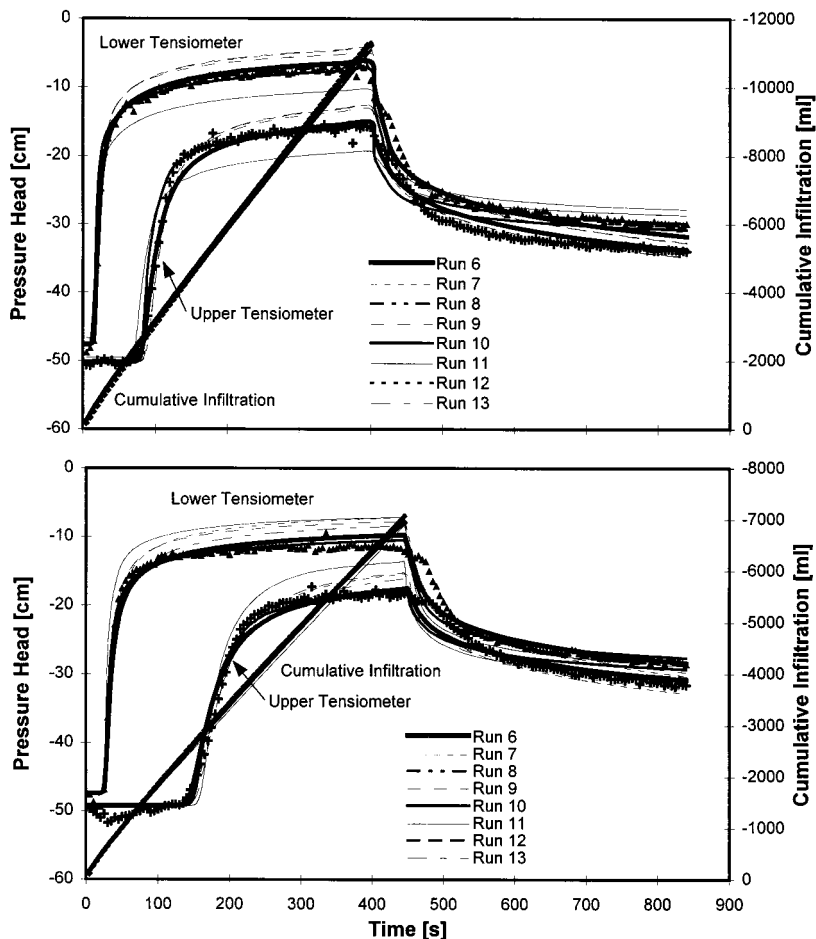


**Figure 9.** Measured and optimized pressure heads and cumulative infiltrations for experiment 1 (top) and experiment 2 (bottom) during both infiltration and redistribution. Hysteresis was considered; the initial condition was assumed to be on a main draining branch of the retention curve.

**Table 7.** Results of Numerical Inversions for Experiment 1 Considering Hysteresis With Initial Conditions Assumed From the Drying Curve

Run	$\Phi$	$\theta_s$ [-]	$\alpha^w$ , cm <sup>-1</sup>	$n$ [-]	$K_s$ , cm s <sup>-1</sup>	$l$ [-]	$k^A$ [-]	$\alpha^d$ , cm <sup>-1</sup>	Rank
6	0.0129	0.522	0.0501	5.37	0.0120	...	...	0.0315	3
7	0.0299	0.580	0.0593	5.36	0.0124	...	...	...	6
8	0.0125	...	0.0520	5.01	0.00863	...	1.63	0.0319	1
9	0.0257	...	0.0607	4.85	0.00820	...	1.83	...	4
10	0.0373	...	0.0406	7.50 <sup>a</sup>	0.0116	7.32	...	0.0290	7
11	0.1033	...	0.0615	6.74	0.0112	10.4	...	...	8
12	0.0127	0.520	0.0469	4.91	0.0120	0.982	...	0.0306	2
13	0.0278	0.568	0.0623	5.39	0.0122	0.0561	...	...	5

<sup>a</sup>Upper parameter constraint.

tribution), including hysteresis, and with the initial condition defined by the drying branch of the retention curve. Only the curves obtained with an independent fit for  $\alpha^w$  and  $\alpha^d$  are given. The retention curves (Figures 11a and 12a), again, show some uncertainty with respect to  $\theta_s$  when this parameter was optimized. The correspondence between wetting branch retention curves for the different inverse solutions is now slightly better than that shown in Figure 10. The wetting branches of the optimized curves are reasonably close to the independently measured curves for the wetting branch. Although the drying retention curves are located higher (with respect to the pressure head axis) than the wetting curves, their shapes are similar. This is due to the assumption that the parameter  $n$  is the same for both wetting and drying [Kool and Parker, 1987]. Given the excellent fit of the pressure head data, and in view of the uncertainty in the description of the second infiltration phase of the experiment, we did not expect that the available data would allow for an independent fit of  $n$  for the wetting and drying branches. Optimized curves were situated between the laboratory wetting and drying branches of the retention curve for most of the pressure head range. The restriction imposed on  $n$  probably caused a relatively poor description of the drying branch of the retention curve as compared to results obtained with the pressure plate method. The pressure plate method resulted in  $n$  values that differed significantly from those obtained with the capillary rise or computer-automated methods. Since the redistribution phase covered only a relatively limited part of the drying branch, with no information on water contents and water fluxes available,  $n$  should be more reflective of the wetting than for the drying branch if indeed Kool and Parker's [1987] model is appropriate for this particular soil.

The hydraulic conductivity  $K(h)$  functions (Figures 11b and 12b) exhibit distinct hysteretic loops. Except for run 8, the optimized  $K(h)$  functions again show better correspondence

between particular branches (wetting or drying) for the different optimizations than those shown in Figure 10b. Optimization run 8 was obtained with the assumption of soil anisotropy. While the vertical saturated conductivity for this curve was estimated to be about 20% lower than for the other parameter combinations (as shown in Figures 11 and 12), the estimated horizontal conductivity was about 10% higher.

In our experiments we obtained, similar to Kodešová *et al.* [1998b], somewhat larger estimates of  $\theta_s$  and  $K_s$  for experiment 1 having a higher applied pressure head as compared to experiment 2. Still, we obtained good agreement between the hydraulic properties obtained from the first and second cone penetrometer experiments. This agreement is especially good for the estimated properties when hysteresis was considered.

## 5. Summary and Conclusions

We have presented a parameter estimation analysis of cone permeameter data for simultaneous determination of the soil water retention and hydraulic conductivity functions characterizing the hydraulic properties of unsaturated soils. We showed that one can estimate not only the wetting branches of the soil hydraulic characteristics from the infiltration part of the experiment but also simultaneously the wetting and drying curves via analysis of both the infiltration and redistribution parts of the test. Hysteresis was described using a relatively simple empirical model, which scales the wetting scanning curves from the main wetting curve and the drying scanning curves from the main drying curve. Drying and wetting curves were characterized with the same parameters,  $n$ ,  $\theta_r$ ,  $\theta_s$ , and  $K_s$ , and with different parameters  $\alpha^d$  and  $\alpha^w$  which we either assumed to be independent, or constrained by the relationship  $\alpha^w = 2\alpha^d$ . Fixing  $\theta_r$  and  $\theta_s$  at reasonable values and optimizing the other parameters resulted in a less satisfactory fit of the measured flow response. To improve the solution,  $\theta_s$  or addi-

**Table 8.** Results of Numerical Inversions for Experiment 2 Considering Hysteresis With Initial Conditions on a Drying Curve

Run	$\Phi$	$\theta_s$ [-]	$\alpha^w$ , cm <sup>-1</sup>	$n$ [-]	$K_s$ , cm s <sup>-1</sup>	$l$ [-]	$k^A$ [-]	$\alpha^d$ , cm <sup>-1</sup>	Rank
6	0.01298	0.450	0.0551	5.69	0.00964	...	...	0.0359	3
7	0.03578	0.544	0.0647	4.22	0.0104	...	...	...	7
8	0.01243	...	0.0569	5.65	0.00790	...	1.36	0.0363	2
9	0.03225	...	0.0685	5.42	0.00793	...	1.47	...	6
10	0.01764	...	0.0445	5.99	0.00947	4.25	...	0.0333	4
11	0.07158	...	0.0675	7.50 <sup>a</sup>	0.0101	2.49	...	...	8
12	0.01194	0.453	0.0402	3.97	0.00980	4.35	...	0.0306	1
13	0.02195	0.592	0.0727	7.19	0.00980	-0.470	...	...	5

<sup>a</sup>Upper parameter constraint.

tional parameters such as the anisotropy coefficient,  $k^A$ , and the pore-connectivity parameter,  $l$ , were optimized. Interestingly, soil anisotropy had the same effect (in terms of the measured or predicted flow response) as increasing  $\theta_s$  or  $l$ . It seems that our results indicate that knowledge of the initial and final water contents of the soil around the screen is necessary to clearly distinguish between the effects of these three parameters on the resulting water flow field. Water content data were not measured in the experimental setup as presented here (or by Gribb [1996] and Gribb et al. [1998]); incorporation of time domain reflectometry (TDR) elements in the cone permeameter could provide the required additional information.

Although it was not possible from the data collected with the current measurements (cumulative infiltration volumes and pressure heads at two positions above the water source) to distinguish between the specific effects of  $\theta_s$ ,  $l$ , and  $k^A$  on the water flow field, the parameters  $\alpha^w$ ,  $\alpha^d$ ,  $n$ , and  $K_s$  were all

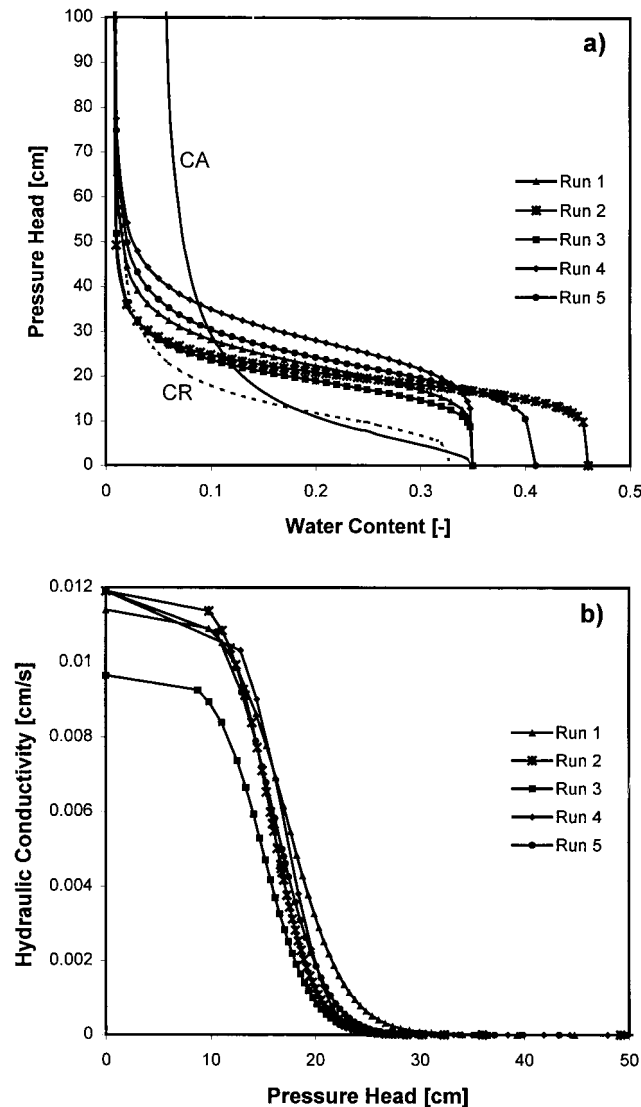


**Figure 10.** (a) Measured and estimated soil water retention and (b) estimated hydraulic conductivity curves using infiltration data of experiment 1 (CR, capillary rise (wetting curve); CA, computer-automated test (wetting curve)).

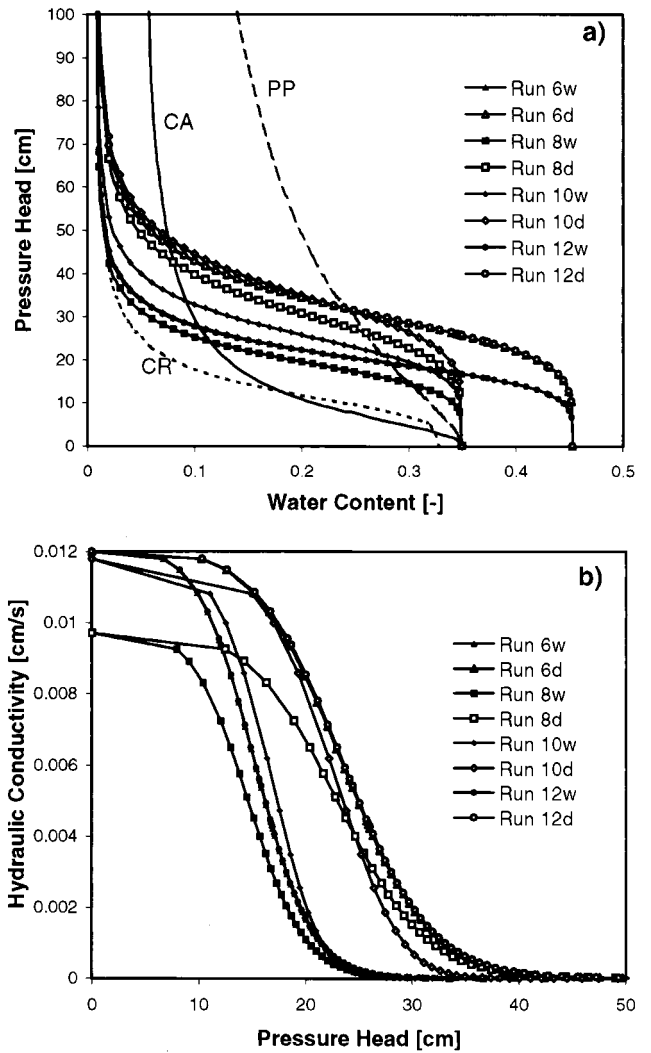


**Figure 11.** (a) Measured and estimated soil water retention and (b) estimated hydraulic conductivity curves using combined infiltration and redistribution data from experiment 1 and considering hysteresis (CR, capillary rise (wetting curve); CA, computer-automated test (wetting curve); PP, pressure plate (drying curve); d, drying; w, wetting).

uniquely estimated and showed a high degree of consistency. We found that the simple hysteretic model was satisfactory for describing differences in wetting and drying behavior observed during this cone experiment. Simultaneous analysis of both infiltration and redistribution, while considering hysteresis in the soil hydraulic properties, increased the identifiability of the optimized parameters with respect to the solution based solely on wetting process data. The estimated soil hydraulic properties estimated from cone permeameter experiments 1 and 2 were similar to each other. The estimated wetting branches of the retention curve compared fairly well with retention curves fitted to results obtained with the capillary rise and computer-automated methods. Failure to similarly describe closely the drying branch obtained using the pressure plate method was attributed to limitations in the implemented hysteresis model which assumes the same  $n$  values for both the wetting and drying branches of the retention curve. The estimated soil saturated hydraulic conductivity compared well with independent estimates.

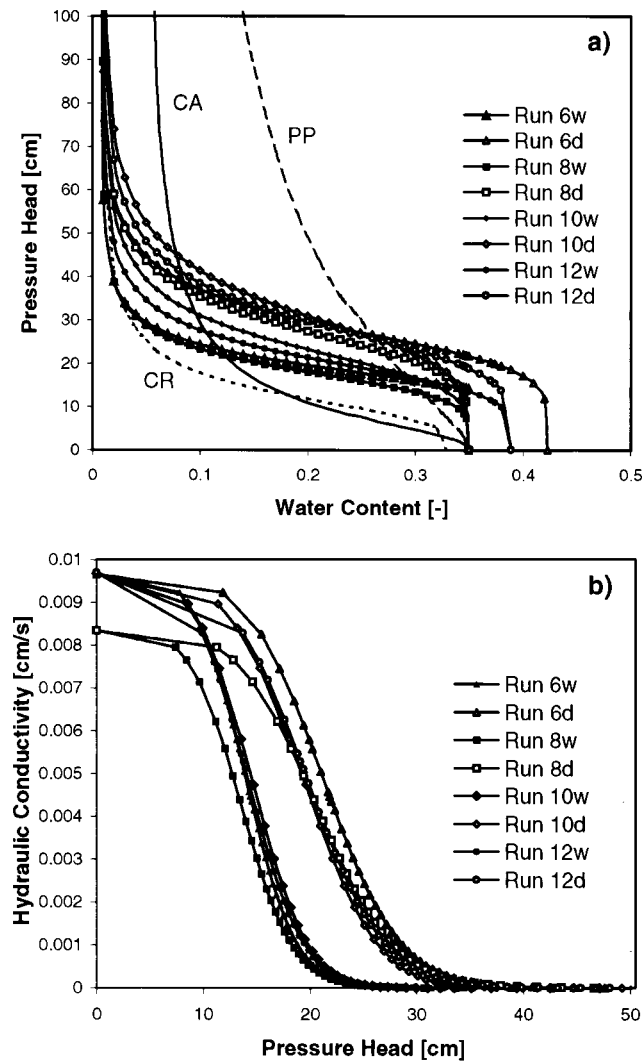


**Figure 12.** (a) Measured and estimated soil water retention and (b) estimated hydraulic conductivity curves using combined infiltration and redistribution data from experiment 2 and considering hysteresis (CR, capillary rise (wetting curve); CA, computer-automated test (wetting curve); PP, pressure plate (drying curve); d, drying; w, wetting).

In this study we analyzed data collected after the cone permeameter was carefully buried in the soil profile to limit the effects of soil disturbance on the optimized soil hydraulic properties. Although *Kodešová et al.* [1998b] investigated the effects of cone placement on optimized soil hydraulic properties and concluded that disturbance had a little impact on the values of the estimated parameters for this particular sandy soil, we believe that additional studies of placement and soil disturbance must be carried out for different soils.

**Acknowledgment.** Thanks are due to reviewers (Jos van Dam and Wolfgang Dürner) for their many useful suggestions and comments.

## References

- Aziz, K., and A. Settari, *Petroleum Reservoir Simulation*, pp. 395–401, Applied Science, Barking, U. K., 1979.
- Bard, Y., *Nonlinear Parameter Estimation*, 341 pp., Academic, San Diego, Calif., 1974.
- Bower, H., and R. C. Rice, A slug test for determining hydraulic conductivity of unconfined aquifers with completely or partially penetrating wells, *Water Resour. Res.*, 12(3), 432–428, 1976.
- Ciollaro, G., and N. Romano, Spatial variability of the soil hydraulic properties of a volcanic soil, *Geoderma*, 65, 263–282, 1995.
- Clausnitzer, V., and J. W. Hopmans, Non-linear parameter estimation: LM\_OPT, general-purpose optimization code based on the Levenberg-Marquardt algorithm, *Land, Air and Water Resour. Pap. 100032*, Univ. of Calif., Davis, 1995.
- Dane, J. H., and S. Hruska, In-situ determination of soil hydraulic properties during drainage, *Soil Sci. Soc. Am. J.*, 47(3), 619–624, 1983.
- Eching, S. O., and J. W. Hopmans, Optimization of hydraulic functions from transient outflow and soil water pressure data, *Soil Sci. Soc. Am. J.*, 57, 1167–1175, 1993.
- Gillham, R. W., A. Klute, and D. F. Heermann, Measurement and numerical simulation of hysteretic flow in a heterogeneous porous medium, *Soil Sci. Soc. Am. J.*, 43(6), 1061–1067, 1979.
- Gribb, M. M., Parameter estimation for determining hydraulic properties of a fine sand from transient flow measurements, *Water Resour. Res.*, 32(7), 1965–1974, 1996.
- Gribb, M. M., J. Šimůnek, and M. F. Leonard, Development of a cone penetrometer method to determine soil hydraulic properties, *J. Geotech. Geoenviron. Eng.*, 124(9), 820–829, 1998.
- Hoa, N. T., R. Gaudu, and C. Thirriot, Influence of the hysteresis effect on transient flows in saturated-unsaturated porous media, *Water Resour. Res.*, 13, 992–996, 1977.
- Hvorslev, M. J., Time lag and soil permeability in ground-water observations, *WES Bull. 36*, U.S. Army Corps of Eng., Vicksburg, Miss., 1951.
- Inoue, M., J. Šimůnek, J. W. Hopmans, and V. Clausnitzer, In-situ estimation of soil hydraulic functions using a multistep soil water extraction technique, *Water Resour. Res.*, 34(5), 1035–1050, 1998.
- Jaynes, D. B., Estimating hysteresis in the soil water retention function, in *Proceedings of the International Workshop on Indirect Methods for Estimating the Hydraulic Properties of Unsaturated Soils*, edited by M. T. van Genuchten et al., pp. 219–232, Univ. of Calif., Riverside, 1992.
- Kaluarachchi, J. J., and J. C. Parker, Effects of hysteresis with air entrapment on water flow in the unsaturated zone, *Water Resour. Res.*, 23(10), 1967–1976, 1987.
- Klute, A., and D. F. Heerman, Soil water profile development under a periodic boundary condition, *Soil Sci.*, 117, 265–271, 1974.
- Kodešová, R., M. M. Gribb, and J. Šimůnek, A new CPT method for estimating soil hydraulic properties, in *Proceedings of the First International Conference on Site Characterization*, vol. 2, edited by P. K. Robertson and P. W. Mayne, pp. 1421–1425, A. A. Balkema, Rotterdam, Netherlands, 1998a.
- Kodešová, R., M. M. Gribb, and J. Šimůnek, Estimating soil hydraulic properties from transient cone permeameter data, *Soil Sci.*, 163(6), 436–453, 1998b.
- Kool, J. B., and J. C. Parker, Development and evaluation of closed-form expressions for hysteretic soil hydraulic properties, *Water Resour. Res.*, 23(1), 105–114, 1987.
- Kool, J. B., and J. C. Parker, Analysis of the inverse problem for transient unsaturated flow, *Water Resour. Res.*, 24(6), 817–830, 1988.
- Kool, J. B., J. C. Parker, and M. T. van Genuchten, Determining soil hydraulic properties from one-step outflow experiments by parameter estimation, I, Theory and numerical studies, *Soil Sci. Soc. Am. J.*, 49, 1348–1354, 1985.
- Kool, J. B., J. C. Parker, and M. T. van Genuchten, Parameter estimation for unsaturated flow and transport models—A review, *J. Hydrol.*, 91, 255–293, 1987.
- Lambe, W. T., Capillary phenomena in cohesionless soils, *Trans. Am. Soc. Civ. Eng.*, 116, 401–423, 1951.
- Luckner, L., M. T. van Genuchten, and D. R. Nielsen, A consistent set of parametric models for the two-phase flow of immiscible fluids in the subsurface, *Water Resour. Res.*, 25(10), 2187–2193, 1989.
- Marquardt, D. W., An algorithm for least-squares estimation of non-linear parameters, *SIAM J. Appl. Math.*, 11, 431–441, 1963.
- Mualem, Y., Modified approach to capillary hysteresis based on a similarity hypothesis, *Water Resour. Res.*, 9(5), 1324–1331, 1973.
- Mualem, Y., A conceptual model of hysteresis, *Water Resour. Res.*, 10(3), 514–520, 1974.
- Mualem, Y., A new model for predicting the hydraulic conductivity of unsaturated porous media, *Water Resour. Res.*, 12(3), 513–522, 1976.

- Mualem, Y., A modified dependent-domain theory of hysteresis, *Soil Sci.*, 137, 283–294, 1984a.
- Mualem, Y., Anisotropy of unsaturated soils, *Soil Sci. Soc. Am. J.*, 48, 505–509, 1984b.
- Mualem, Y., and G. Dagan, A dependent domain model of capillary hysteresis, *Water Resour. Res.*, 11(3), 452–460, 1975.
- Mualem, Y., and H. J. Morel-Seytoux, Analysis of a capillary hysteresis model based on a one-variable distribution function, *Water Resour. Res.*, 14(4), 605–610, 1978.
- Nielsen, D. R., and L. M. Luckner, Theoretical aspects to estimate reasonable initial parameters and range limits in identification procedures for soil hydraulic properties, in *Proceedings of the International Workshop on Indirect Methods for Estimating the Hydraulic Properties of Unsaturated Soils*, edited by M. T. van Genuchten et al., pp. 147–160, Univ. of Calif., Riverside, 1992.
- Ray, R. P., and K. B. Morris, Automated laboratory testing for soil/water characteristic curves, in *Proceedings of 1st International Conference on Unsaturated Soils*, vol. 2, edited by E. Alonso and P. Delage, pp. 236–241, A. A. Balkema, Rotterdam, Netherlands, 1994.
- Reynolds, W. D., Unsaturated hydraulic conductivity: Field measurement, in *Soil Sampling and Methods of Analysis*, edited by M. R. Carter, pp. 633–644, Lewis, New York, 1993.
- Royer, J. M., and G. Vachaud, Field determination of hysteresis in soil-water characteristics, *Soil Sci. Soc. Am. J.*, 39(2), 221–223, 1975.
- Russo, D., W. A. Jury, and G. L. Butters, Numerical analysis of solute transport during transient irrigation, 1, The effect of hysteresis and profile heterogeneity, *Water Resour. Res.*, 25(10), 2109–2118, 1989.
- Santini, A., N. Romano, G. Ciollaro, and V. Comegna, Evaluation of a laboratory inverse method for determining unsaturated hydraulic properties of a soil under different tillage practices, *Soil Sci.*, 160, 340–351, 1995.
- Scaturro, D. M., Evaluation of multi-level direct push sampling for hydraulic conductivity analysis, M. S. thesis, Univ. of S. C., Columbia, 1993.
- Scott, P. S., G. J. Farquhar, and N. Kouwen, Hysteresis effects on net infiltration, in *Advances in Infiltration*, Publ. 11-83, pp. 163–170, Am. Soc. of Agric. Eng., St. Joseph, Mich., 1983.
- Šimůnek, J., and M. T. van Genuchten, Parameter estimation of soil hydraulic properties from the tension disc infiltrometer experiment by numerical inversion, *Water Resour. Res.*, 32(9), 2683–2696, 1996.
- Šimůnek, J., and M. T. van Genuchten, Estimating unsaturated soil hydraulic properties from multiple tension disc infiltrometer data, *Soil Sci.*, 162(6), 383–398, 1997.
- Šimůnek, J., M. Šejna, M., and M. T. van Genuchten, The HYDRUS-2D software package for simulating water flow and solute transport in two-dimensional variably saturated media, version 1.0, *IGWMC - TPS 53*, Int. Ground Water Modeling Cent., Colo. School of Mines, Golden, 1996.
- Šimůnek, J., O. Wendroth, and M. T. van Genuchten, A parameter estimation analysis of the evaporation method for determining soil hydraulic properties, *Soil Sci. Soc. Am. J.*, 62(4), 894–905, 1998.
- Singleton, J. E., Hydraulic characteristics of a laboratory aquifer, M. S. thesis, Univ. of S. C., Columbia, 1997.
- Topp, G. C., Soil-water hysteresis measured in a sandy loam and compared with the hysteretic domain model, *Soil Sci. Soc. Am. Proc.*, 33, 645–651, 1969.
- Vachaud, G., and J.-L. Thony, Hysteresis during infiltration and redistribution in a soil column at different initial water contents, *Water Resour. Res.*, 7(1), 111–127, 1971.
- van Dam, J. C., J. N. M. Stricker, and P. Droogers, Inverse method for determining soil hydraulic functions from one-step outflow experiment, *Soil Sci. Soc. Am. Proc.*, 56, 1042–1050, 1992.
- van Dam, J. C., J. N. M. Stricker, and P. Droogers, Inverse method to determine soil hydraulic functions from multistep outflow experiment, *Soil Sci. Soc. Am. Proc.*, 58, 647–652, 1994.
- van Genuchten, M. T., A closed-form equation for predicting the hydraulic conductivity of unsaturated soils, *Soil Sci. Soc. Am. J.*, 44, 892–898, 1980.
- van Genuchten, M. T., Non-equilibrium transport parameters from miscible displacement experiments, *Res. Rep. 119*, U.S. Salinity Lab., U.S. Dep. of Agric., Riverside, Calif., 1981.
- van Genuchten, M. T., F. J. Leij, and S. R. Yates, The RETC code for quantifying the hydraulic functions of unsaturated soils, *EPA/600/2-91-065*, US EPA, Off. of Res. and Dev., U.S. Environ. Prot. Agency, Washington, D. C., 1991.
- Vogel, T., K. Huang, R. Zhang, and M. T. van Genuchten, The HYDRUS code for simulating one-dimensional water flow, solute transport, and heat movement in variably-saturated media, version 5.0, *Res. Rep. No 140*, U.S. Salinity Lab., U.S. Dep. of Agric., Riverside, Calif., 1996.
- Watson, K. K., R. J. Reginato, and R. D. Jackson, Soil water hysteresis in a field soil, *Soil Sci. Soc. Am. Proc.*, 39, 242–246, 1975.
- Yeh, W. W.-G., Review of parameter identification procedures in groundwater hydrology: The inverse problem, *Water Resour. Res.*, 22(2), 95–108, 1986.
- Znidarčič, D., T. Ilangasekare, and M. Manna, Laboratory testing and parameter estimation for two-phase flow problems, in *Geotechnical Engineering Congress*, edited by F. G. McClean et al., *Geotech. Spec. Publ. 27(2)*, pp. 1089–1099, 1991.

M. M. Gribb and R. Kodešová, Department of Civil and Environmental Engineering, University of South Carolina, Columbia, SC 29208.

J. Šimůnek and M. T. van Genuchten, U.S. Salinity Laboratory, ARS, USDA, 450 W. Big Springs Rd., Riverside, CA 92507. (jsimunek@ussl.ars.usda.gov)

(Received March 6, 1998; revised December 3, 1998; accepted December 7, 1998.)

